Spatial Modulation of Vibrational and Luminescence Properties of Monolayer MoS_2 Using a GaAs Nanowire Array

Akshay Balgarkashi, Valerio Piazza, Jakub Jasiński, Riccardo Frisenda, Alessandro Surrente, Michał Baranowski, Mirjana Dimitrievska, Didem Dede, Wonjong Kim, Lucas Güniat, Jean-Baptiste Leran, Andres Castellanos-Gomez, Paulina Plochocka, and Anna Fontcuberta i Morral, *Member, IEEE*

***Abstract*— The integration of transition-metal dichalcogenides (TMDs) with non-planar substrates such as nanopillars provides a way to spatially modify the optical properties mainly through the localized strain. Similar studies to date have utilized insulating SiO_2 nanopillars. Here, we combine monolayer MoS_2 with free standing GaAs nanowires (NWs), in views of coupling their semiconducting properties. We find that monolayer MoS_2 exhibits three different configurations: pierced, wrapped and tent-like. We demonstrate how to identify the configurations by optical microscopy and elucidate the impact on the vibrational and luminescence characteristics by confocal spectroscopy mapping. In particular, we highlight the increase of intensity and shift due to the photonic properties of nanowires and increase in dielectric screening associated with the GaAs NW. This work signifies the first step towards the use of vertical III-V NW arrays as a versatile platform for spatially engineering the optical properties of TMDs.**

***Index Terms*— Nanowires, photoluminescence, Raman spectroscopy, transition-metal dichalcogenides.**

Manuscript received 1 December 2021; revised 13 March 2022; accepted 4 April 2022. Date of publication 14 April 2022; date of current version 28 July 2022. This work was supported in part by the Swiss National Science Foundation (SNSF) under Project 196948, in part by the European Union's Horizon 2020 Research and Innovation Program under the Marie Skłodowska-Curie under Grant 765075, in part by Project LIMQUET, in part by the European Research Council (ERC) under the European Union's Horizon 2020 Research and Innovation Program under Grant 755655, and in part by ERC-StG 2017 Project 2D-TOPSENSE. The work of Michał Baranowski was supported by the National Science Centre Poland within the SONATA BIS Program under Grant 2020/38/E/ST3/00194. *(Corresponding author: Anna Fontcuberta i Morral.)*

Akshay Balgarkashi, Valerio Piazza, Mirjana Dimitrievska, Didem Dede, Lucas Güniat, and Jean-Baptiste Leran are with the Laboratory of Semiconductor Materials, Institute of Materials, École Polytechnique Fédérale de Lausanne (EPFL), 1015 Lausanne, Switzerland (e-mail: akshay.balgarkashi@epfl.ch; valerio.piazza@epfl.ch; mirjana.dimitrievska@epfl.ch; didem.dede@epfl.ch; lucas.guniat@epfl.ch; jean-baptiste.leran@epfl.ch).

Jakub Jasiński, Alessandro Surrente, and Michał Baranowski are with the Department of Experimental Physics, Faculty of Fundamental Problems of Technology, Wrocław University of Science and Technology, 50-370 Wrocław, Poland (e-mail: jakub.jasinski@pwr.edu.pl; alessandro.surrente@pwr.edu.pl; michal.baranowski@pwr.edu.pl).

Riccardo Frisenda and Andres Castellanos-Gomez are with Materials Science Factory, Instituto de Ciencia de Materiales de Madrid (ICMM-CSIC), 28049 Madrid, Spain (e-mail: riccardo.frisenda@csic.es; andres.castellanos@csic.es).

Wonjong Kim was with the Laboratory of Semiconductor Materials, Institute of Materials, EPFL, 1015 Lausanne, Switzerland. He is now with ASM International, 3001 Leuven, Belgium (e-mail: wonjong.kim@asm.com).

Paulina Plochocka is with the Department of Experimental Physics, Faculty of Fundamental Problems of Technology, Wrocław University of Science and Technology, 50-370 Wrocław, Poland, and also with the Laboratoire National des Champs Magnétiques Intenses, UPR 3228, CNRS-UGA-UPS-INSA, 31400 Toulouse, France (e-mail: paulina.plochocka@lncmi.cnrs.fr).

Anna Fontcuberta i Morral is with the Laboratory of Semiconductor Materials, Institute of Materials, École Polytechnique Fédérale de Lausanne (EPFL), 1015 Lausanne, Switzerland, and also with the Institute of Physics, EPFL, 1015 Lausanne, Switzerland (e-mail: anna.fontcuberta-morral@epfl.ch).

This article has supplementary material provided by the authors and color versions of one or more figures available at https://doi.org/10.1109/JQE.2022.3167480.

Digital Object Identifier 10.1109/JQE.2022.3167480

I. Introduction

TWO-DIMENSIONAL materials have emerged as a promising new platform for optoelectronic applications such as transistors [1], solar cells [2], detectors [3] and single photon emitters [4]–[6]. Monolayer (ML) transition-metal dichalcogenides (TMDs), in particular, show interesting optical, electronic and mechanical properties, including direct bandgap [7], large exciton binding energies [8] and spin and valley-selective optical transitions [9]. The ease of various transfer methods [10] has enabled integration with a high variety of substrates, including non-planar surfaces [5], [11]–[15].

The attributes of the interface with the substrate exert a direct influence on the ML-TMD characteristics, due to the monolayer character. For example, non-planar substrates spatially modulate the strain. This modulation can be exercised using different nanostructures such as nanoparticles and nanopillar/NWs [12], [14], [15]. In addition, Fermi level alignment with the substrate alters the carrier concentration in TMDs through charge exchange [16]. This provides the ability to modulate the carrier concentration in TMDs by changing the substrate characteristics.

The integration of ML-TMDs with patterned non-planar substrates constitutes an appealing platform to engineer ML-TMDs. In particular, it has been shown that nanopillars induce a localized strain, resulting into a local change of the band structure. This can either induce exciton funneling at low temperatures [17] or efficient exciton to trion conversion at room temperature [18] in the direction of the nanopillar tip, where the strain is maximum. This enables efficient charge collection, desirable for bright single photon emission. Following this strategy, nanopillars were used to controllably create single photon emitters in ML-TMDs such as

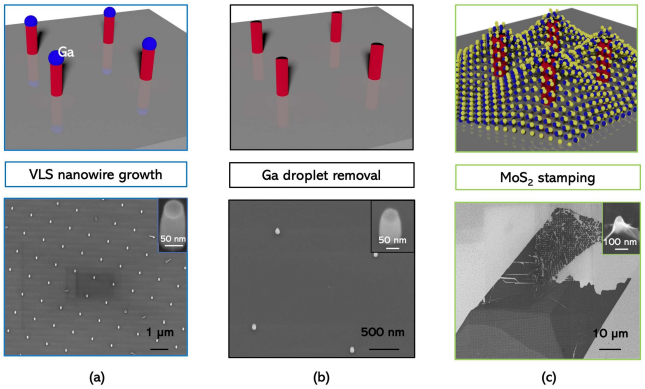

Fig. 1. Schematic (top) and corresponding SEM image (bottom) of a GaAs NW array (a) after growth, (b) after Ga droplet removal and (c) after MoS_2 flake stamping.

WSe_2 [5], [13]. To the best of our knowledge, most works have used insulating SiO_2 nanopillars. The SiO_2 is not ideal in this application since it contains trapped charges, which creates a fluctuating dielectric environment. This causes spectral and intensity fluctuations in the optical emission of the localized emitters [19]. Epitaxially grown III-V substrates, on the other hand, can provide a cleaner charge environment at the interface with ML-TMDs due to the absence of trapped charges [19]. In the form of nanowire (NW) arrays, III-V substrates can be used to create localized strain in TMDs. Additionally, the aspect ratio and pitch of the NW arrays can be modulated to systematically vary the strain. In addition, doping of III-V NWs provides an additional path towards the modification of the potential landscape in the ML-TMD [20], [21].

In this work, we combine ML-MoS_2 with GaAs NWs on silicon. By performing optical and atomic force microscopy maps on the same regions we identify three different configurations that the ML-MoS_2 adopts. We then acquire Raman and photoluminescence (PL) spectroscopy maps to elucidate the effect of NWs on the properties of the ML-MoS_2.

II. Results and Discussion

We start by providing an overview of the studied system. Fig. 1 shows a schematic drawing and the corresponding scanning electron microscope (SEM) image of a GaAs NW array at each stage of the sample preparation. GaAs NW arrays were grown by molecular beam epitaxy (MBE) on Si substrates, following [22], [23]. Fig. 1(a) corresponds to the NW array after growth. The NWs are arranged in a square lattice of 1.6 μm side. The measured diameter and height of the NWs are $\sim$55 nm and 300 nm respectively. The inset highlights a representative GaAs NW with Ga droplet on top. Prior to flake transfer, the Ga droplets were etched away in 37% HCl solution (fig. 1(b)). We feature a representative single NW in the inset of fig. 1(b) where the Ga droplet is clearly absent. The GaAs NWs were exposed to atmospheric environment less than 2 days prior to the ML transfer. Based on previous publications on GaAs epilayer, we expect formation of ultra-thin GaOx (1 nm around) on the lateral surface [24]. ML MoS_2 flake was then transferred on the GaAs NW array. Fig. 1(c) depicts the SEM image of the NW array after transfer of a ML MoS_2. The inset shows a single NW with a flake on top. In this particular case, the flake is suspended on the NW tip forming a tent-like structure. More details on NW growth and flake transfer can be found in the Methods section. Monolayers were identified from the optical contrast and from the optical transmission of the flake prior to transfer and confirmed by Raman spectroscopy. The frequency difference between the in-plane and out-of-plane Raman peaks for a ML was found to be 20 cm^{-1} (Supplementary information fig. SI-1) in agreement with previous studies [25].

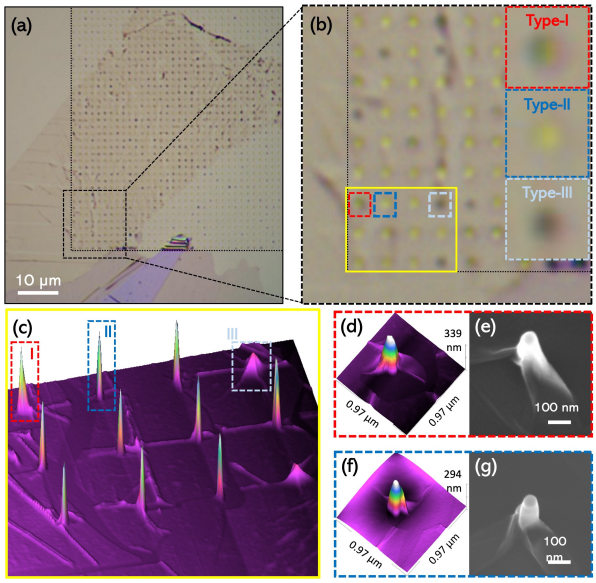

Fig. 2. (a) Bright-field optical image of the MoS_2 flake after transfer to GaAs NW array. (b) Magnified optical image from the bottom left corner of the NW array as indicated in (a). The insets show magnified views of NWs with three different types of optical contrast labeled as type-I, II and III. (c) A 3-D AFM image from the area denoted by yellow box in (b). The dotted rectangles denote the three different configurations of the flake on NWs. 3-D AFM and SEM images, respectively, of (d)-(e) type-I and (f)-(g) type-II configurations as indicated by red and blue dotted rectangles in (c).

A. Configuration Identification

We turn now to the identification of the configurations adopted by the ML-MoS_2 on the NWs. Fig. 2(a) shows an overview bright-field optical image of the monolayer MoS_2 flake on NWs. A magnified optical image from the bottom left corner of the array is shown in fig. 2(b), which is marked by a black dashed square in (a). The dotted lines in fig. 2(b) mark the edge of the NW array. Three different optical contrasts were identified. We have highlighted the three representative examples with colored dashed lines and further magnified them in the inset of fig. 2(b). We label them type-I, II and III. They are respectively characterized by a half dark/bright, full bright and full dark spot.

In order to understand the topology of the flake on the NW array, the sample was studied by atomic force microscopy (AFM) and SEM. Fig. 2(c) shows a three-dimensional view of the AFM image taken from the bottom left corner of the NW array identified with a yellow box. The AFM measurement shown in fig. 2(c) clearly reveals

that the flake does not lie identically on all NWs. Type-I and II configurations appear spiky, while configuration III exhibits a shorter tent-like shape. The latter corresponds to shorter NW structures that might have been broken during the transfer process. More details of type-III NWs can be found in Supplementary information fig. SI-2. A closer look on the type-I and type-II configurations is shown in figs. 2(d)-(g), represented by 3-D AFM and SEM images. For the type-I configuration, the flake is conformal to the NWs as evident in figs. 2(d) and (e). Moreover, the flake is disconnected from rest of the flake around the NW on most sides. The flake tends to wrap around the NW.

3-D AFM and SEM images of type I and II configurations are shown for direct comparison in figs. 2(d) and (f), and (e) and (g), respectively. The flake appears to be pierced by the NWs in the case of type-II configuration. This is evident in the SEM image of fig. 2(g). The pierced flake mostly lies close to the bottom of the NW. We observe a clear correlation between the optical contrast and the flake topology on a NW. The optical contrast found in the optical microscopy can be used to reliably identify the flake configuration on the NWs. Statistics on a small region of the array is provided in Supplementary Information fig. SI-3. Most of the NWs exhibit type-II (pierced) configuration while type-I and III constitute a small proportion of the NWs in the array. Out of 124 NWs, on average type-I and III constitute 10% each, while the rest are found to be type-II.

In the areas between the NWs, the flake lies in contact with the substrate. We think this is because of the large NW pitch, in contrast to the reduced NW diameter. In some regions, the flake exhibits ripple-like lines which may have been produced during the transfer process [11]. We also identify some regions of the flake in between the NWs which appear to be folded. Borders of folded regions may appear as faint black lines in the optical image in fig. 2(b). We think that folding may have occurred during the transfer process. For further confirmation, a representative SEM image of a folded region is provided in fig. SI-4. For future studies, we suggest to explore the transfer of wafer size monolayers in the attempt of improving the controllability of the ML-on-NW configurations throughout the array [26], [27].

B. Optical Spectroscopy

We now address the effect of the monolayer MoS_2 configuration on the vibrational and luminescence properties. Several aspects may be of influence, such as strain and charge transfer/interface with the substrate [12], [28]. Raman spectroscopy is a non-destructive tool to study strain and electronic charge effects in 2-D materials [29], [30]. In particular, it is well-known that the in-plane Raman mode (E2g) of MoS_2 is sensitive to strain [31] while the out-of-plane Raman mode (A_{1g}) is more responsive to variations in the carrier concentration [32].

Fig. 3 presents the Raman mapping results of the sample shown in Fig. 2. Fig. 3(a) corresponds to the optical image of the region investigated. The numbers correspond to representative points where the spectra were extracted. Fig. 3(b) displays these selected Raman spectra, which have

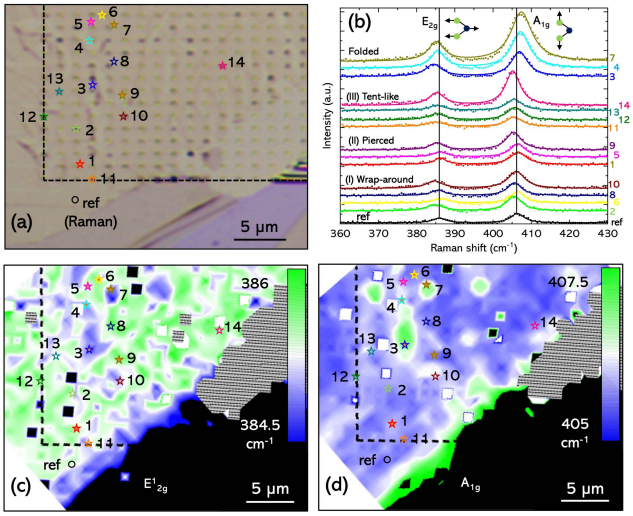

Fig. 3. (a) Optical image of region of the MoS_2 flake on NWs mapped in Raman measurements. (b) Raman spectra corresponding to the points indicated in the optical image in (a). The spectra are grouped according to the flake configuration labeled as "folded" (points 3, 4 and 7), "tent-like" (points 11, 12, 13 and 14), "pierced" (points 1, 5, 9) and wrap-around (points 2, 6, 8 and 10). "ref" indicates a reference point on the ML outside the array. (c) and (d) show the Raman maps representing E^1_{2g} and A_{1g} peak positions acquired from the area depicted in the optical image. The black dashed lines in (a), (c) and (d) indicate edges of the NW array.

been grouped according to their configuration. These were identified from the optical contrast as discussed in the previous section. The groups are labeled as "folded" (points 3, 4 and 7), type III "tent-like" (points 11, 12, 13 and 14), type II "pierced" (points 1, 5, 9) and type I wrap-around (points 2, 6, 8 and 10), respectively. As a reference, the Raman spectrum acquired from a point on the ML outside the NW array is also provided. This point is denoted as "ref" in fig. 3. Figs. 3(c) and (d) correspond to the maps of E^1_{2g} and A_{1g} Raman peak positions acquired from the same area as the optical image. The black dashed lines indicate the edges of the NW array.

We now compare each group of spectra with the reference. The symbols in each spectrum indicate the raw data and solid lines are the corresponding Lorentzian fits. Results of the fits have been listed in the Supplementary information Table-1. For the reference spectrum, the E^1_{2g} and A_{1g} peak positions are located at 385.9 and 406.4 cm^{-1} respectively with a frequency difference, $\Delta f \sim 20.5$ cm^{-1} compatible with a monolayer MoS_2 [25]. Spectra from points 3, 4 and 7 corresponds to regions where the MoS_2 has been folded. The spectra exhibit a redshift of the E^1_{2g} mode ($\sim$1.5 cm^{-1}) and a blueshift of the A_{1g} mode ($\sim$1 cm^{-1}). The frequency difference between the two modes at these points was found to be 22.5 cm^{-1}. Additionally, enhanced intensity of the Raman peaks is observed for this configuration, when compared to the reference. Both of these factors are consistent with a multilayer behavior [25], [33]. Such regions can also be identified in the Raman maps of fig. 3(c) and (d) with a blue and green texture which indicates an increase in Δf.

The second group of spectra represents a "tent-like" configuration. The Raman spectra at these points (11, 12, 13 and 14) are characterized by a downshift in both the E^1_{2g}

and A_{1g} modes. The E^1_{2g} mode redshifts by 0.7 cm^{-1}. This is attributed to a tensile strain induced by the NW in the ML flake. In this configuration, the flake is supported by the NW and forms a tent. Such tent-like structures on SiO_2 nanopillars have been shown to induce a tensile strain in the monolayer [12]. In addition, the A_{1g} mode also redshifts by 0.9 cm^{-1}. We attribute this to either an unintentional doping or charge transfer in the flake from the underlying substrate [34].

In the third group of spectra (1, 5 and 9), the flake has been "pierced" by the NWs. The Raman peak positions in spectra from points 1 and 5 are similar to the reference and do not show any considerable shift. Only in the case of point 9, a small redshift in both the Raman modes is observed. Similarly, for the fourth group of spectra (points 2, 6, 8 and 10) labels as "wrap-around," the shift at each point is slightly different. For instance, points 2 and 10 are characterized by a redshift of the E^1_{2g} ($\sim$1 cm^{-1}) mode compared to the reference, whereas for points 6 and 8, the E^1_{2g} peak position is similar to the reference. In case of the A_{1g} mode, points 2 and 8 show a redshift ($\sim$0.8 cm^{-1}) in comparison to the reference peak, while for points 6 and 10, no considerable shift in the A_{1g} peak position is observed. From the peak shifts observed above, the Raman spectra for "pierced" and "wrap-around" configurations do not show a clear trend. There is a point-to-point variation even within these two groups. This is in contrast to the "folded" and "tent-like" configurations which showed a clear multilayer behavior and redshift in both the Raman peaks, respectively. This is an interesting observation which we attribute to the fact that the "pierced" and "wrap-around" configurations are more disordered compared to the other two configurations. For example, when a flake is pierced by the NW, it can either be fully or partially pierced. A fully pierced flake will then lie flat on the substrate around the NW. For a partially pierced flake, the topography will be different from NW to NW depending on how the flake gets pierced.

We thus note that the strain profile in each case will be complex and can either be partially or fully relaxed implying non-uniform shifts in the E^1_{2g} peak. A similar reasoning can be made in case of the wrap-around configuration with variations in how the flake wraps around the NW. Likewise, the shifts in A_{1g} peak will also depend on how the flake interacts with the substrate. The flake is either in contact with the SiO_2 substrate or GaAs NWs or both. This again implies non-uniform shifts in the A_{1g} peak. At this point, individual effects for these two configurations cannot be distinguished. Although variations in the Raman peaks, in general, provide a proof of strain and charge transfer induced due to coupling between the ML MoS_2 and GaAs NWs.

We now turn to correlate the flake configuration with the luminescence properties using confocal PL spectroscopy. Fig. 4 presents the confocal PL mapping of the ML MoS_2 on GaAs NWs. Fig. 4(a) shows an optical image of the region mapped in the PL measurements. Fig. 4(b) and (c) show the PL energy and intensity maps, respectively, corresponding to the area shown in (a). The dashed black lines indicate edges of the NW array. Fig. 4(d) shows the PL spectra extracted from the points indicated in figs. 4(a) and (b) and correspond

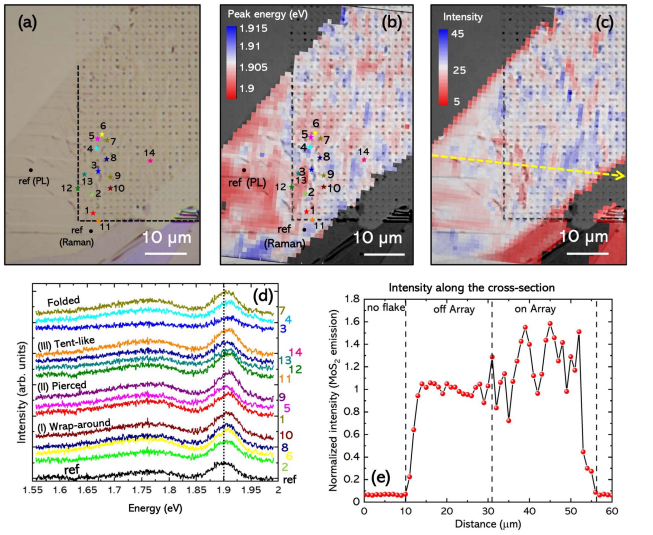

Fig. 4. (a) An optical image of the region mapped in the PL measurements. (b) and (c) show the PL energy and intensity maps, respectively, corresponding to the area shown in (a). The dashed black lines indicate edges of the NW array. (d) PL spectra extracted from the points indicated in (a) and (b), corresponding to the points used in the Raman measurements except the reference. A new reference point is taken for PL spectral comparison, denoted as "ref (PL)." (e) An intensity linescan across the cross-section indicated by a dashed yellow line in (c).

to the points studied in the Raman measurements except for the reference. The reference point on the ML used for Raman spectral comparison (denoted as "ref (Raman)") is close to the edge of the NW array. The PL emission peak from the ML shows a blueshift as we approach the edges of the NW array. An additional reference point is taken far away from the array, denoted as "ref (PL)."

We now compare the PL spectra from MoS_2 on NWs with the reference. As shown in fig. 4(d), the PL spectra are characterized by two main features: a dominant peak centered around 1.9 eV and a broad band in the range of 1.6-1.85 eV. The peak at 1.9 eV is attributed to excitonic emission in ML MoS_2 [35]. The PL emission shows a blueshift of 10-15 meV throughout the whole nanowire area, i.e., independently of the configurations of the ML on top of the NWs, in comparison to the reference. The origin of this blueshift will be discussed in detail below. The broad emission band in the range of 1.6-1.85 eV is attributed to the L-band emission caused by the existence of passivated S-vacancies [36]. S-vacancies in exfoliated single layers of MoS_2 are usually passivated by oxygen atoms which are present either as part of adsorbates or as substitutional atoms [32]. In our case, this band is observed in all PL spectra, without any changes between the ML MoS_2 on NWs or reference.

The luminescence properties of monolayer 2-D materials can be affected due to (i) strain [37], (ii) charge transfer [16], (iii) defect passivation [38] and (iv) dielectric screening [39]. Below we make a systematic discussion on how these effects might contribute to the origin of the blue shift of 1.9 eV PL peak observed in our case.

1) Strain and Charge Transfer: We observe only a small shift of the E^1_{2g} and A_{1g} Raman modes in the ML MoS_2 on NWs. This indicates a marginal effect of strain and doping

on the PL spectra of ML MoS_2 on NWs. However, considering that there is no systematic trend in the shift of the Raman peaks in the ML MoS_2 on NWs (fig. 3), it is unlikely that this is the main cause of the consistent blue shift of the 1.9 eV peak that is observed in ML MoS_2 on NWs.

2) Defect Passivation: The physical adsorption of water and oxygen molecules at S-vacancies on MoS_2 may lead to passivation of defects and introduce p-type doping compared to ideal MoS_2 surface [40]. This leads to a trion to exciton conversion and could result in a blueshift of the PL peak. A blueshift of 40 meV is observed even for a thin layer of adsorbates and is typically followed by an enhancement in the PL intensity [41]. Considering that S-vacancies have already been passivated in our sample, based on the appearance of L-band [32] in PL spectra, and there is no change in the shape, intensity or position of the L-band between the reference and the ML MoS_2 on NWs, we can exclude this effect as a reason for the blueshift of the PL emission peak.

3) Dielectric Screening: Engineering the surrounding dielectric environment can also modify the PL emission in ML-TMDs [39]. For example, the dielectric constant of the environment has a strong effect on the exciton binding energy [38]. PL blueshifts up to 40 meV were observed for the excitonic peaks by varying the effective dielectric constant from 2 to 33 by Lin *et. al.* [38]. Additionally, the trion/exciton intensity ratio can also be tuned by an order of magnitude. Fig. SI-6 (a) and (b) present the results of a Lorentzian peak fitting to the PL spectra of monolayer MoS_2 on SiO_2 (reference) and GaAs, respectively. The two Lorentzians account for the neutral A-exciton peak and the trion peak. The trion to A-exciton intensity ratio extracted from the fitting is 1.27 and 0.45 for SiO_2 and GaAs, respectively. This induces an overall blueshift in the PL emission peak of 15 meV from 1.896 eV to 1.911 eV from SiO_2 to GaAs. Based on these observations, one could attribute the blueshift observed here to an enhanced dielectric screening of the Coulomb potential due to the high dielectric constant of GaAs ($\varepsilon = 12.9$) [42], which is almost four times that of SiO_2 ($\varepsilon = 3.9$) [43]. This is consistent with the prior work of Lin et. al. [38]. A further confirmation of this is provided by PL measurements on ML WSe_2 on SiO_2, planar GaAs and GaAs NW substrates (Supplementary information fig. SI-5) where we also see a blueshift in the excitonic emission peak of ML WSe_2. Considering that Lin et. al. [38] have used non-ionic liquids as the dielectric environment to avoid the effects of strain and doping, in our case, we need to take in account the effect of substrate in terms of strain and doping on the PL spectra. As discussed previously, observation of no systematic trend in shift of Raman peaks in ML MoS_2 on NWs indicates only a marginal effect of strain and doping, respectively. Thus, we believe the dielectric screening effect should be dominant in blueshift of the PL emission.

The PL intensity map in fig. 4(c) shows an overall increase in the emission intensity on the NWs compared to the planar region. To further illustrate this in a quantitative manner, fig. 4(e) provides an intensity linescan across the cross-section indicated by a dashed yellow line in (c). The three regions are denoted as no flake, off array and on array. The emission intensity is normalized to the off-array part of the ML. No emission is observed in the absence of a ML. As we approach the ML flake, the emission intensity on the NW array is almost twice the emission intensity off array. We attribute this to the photonic effect of NWs which enhances the brightness around the NWs [44]–[46]. This photonic enhancement effect can be tuned further by optimizing the aspect ratio of the NWs [47].

III. Conclusion

In conclusion, we have successfully demonstrated the combination of a monolayer MoS_2 with a GaAs NW array. Detailed structural studies reveal different configurations of the flake on NWs. We evidence variations in the vibrational properties of the monolayer as an effect of strain and charge transfer due to the NWs. The luminescence shows a blueshift of the PL emission peak as a result of enhanced dielectric screening due to GaAs NWs. This provides a proof-of-concept to combine monolayer TMDs with III-V NWs and opens up possibilities to engineer the strain and enhance light extraction from monolayer TMDs.

A. Methods

1) Growth: Thermally oxidized Si substrates (15 nm SiO_2) were patterned using e-beam lithography. The substrates were etched in a 1% HF solution to remove the native oxide within the nanoholes prior to loading into the MBE growth chamber. Ga droplets were selectively deposited into the nanoholes for 10 minutes. These droplets serve as catalysts for the growth of GaAs NWs. Nanowires are then grown by the vapor-liquid-solid (VLS) mechanism for 10 minutes under Ga and As_4 fluxes of 1.4 $\times$ 10-7 Torr and 2 $\times$ 10-6 Torr, respectively. This corresponds to a GaAs planar growth rate of 1 Å/s. The morphology of nanowires is studied using a Zeiss Merlin scanning electron microscope (SEM) and a Bruker FastScan atomic force microscope (AFM) in non-contact mode. The crystal structure of the nanowires is characterized predominantly by zincblende (ZB) phase. The nanowires luminesce around 1.5 eV at low temperature, which does not interfere with the signal investigated here. Details on the structure and optical properties can be found in a previous publication [48].

2) Flake Transfer: MoS_2 flakes were obtained by mechanical exfoliation from a natural molybdenite crystal from Moly Hill mine (Quebec, Canada) on a Gel-Film (WF x4 6.0 mil) supplied by Gel-Pak®. A monolayer MoS_2 flake was deterministically transferred to a NW array substrate using an all-dry viscoelastic stamping process [49]. The flake exfoliated on a Gel-Film film is attached to a glass slide and the glass slide is used as a stamp. The stamp is first aligned with the NW array and then brought in contact using a Z-axis manipulation stage. Following this, a cotton bud is used to gently press the Gel-Film stamp onto the array.

3) Characterization: For optical spectroscopy, the samples are mounted on the cold finger of a helium flow cryostat. The cryostat is bolted to computer controlled, motorized X-Y translation stages, which allow two-dimensional in-plane motion. The position of the stages is controlled with micrometer screws, either manually or by automatized stepper motors. Programmable automatic motors allow for mapping

measurements, by scanning the sample surface step by step. The PL and Raman measurements were performed using either a CW solid state laser emitting at 405 nm or 532 nm. The excitation beam was focused on the sample by a 50x microscope objective with a numerical aperture of 0.55, giving a spot size of approximately 1 μm. The excitation laser power was kept below 100 μW to avoid heating effects. For PL mapping, the signal was detected in a confocal configuration to improve the spatial resolution. The emitted PL or Raman signal was collected through the same objective and redirected to a spectrometer equipped with a liquid nitrogen-cooled charge-coupled device camera.

Additional data is provided in the *Supplementary Information*.

REFERENCES

[1] B. Radisavljevic, A. Radenovic, J. Brivio, V. Giacometti, and A. Kis, "Single-layer MoS_2 transistors," *Nature Nanotechnol.*, vol. 6, no. 3, pp. 147–150, Mar. 2011.

[2] O. Lopez-Sanchez, D. Lembke, M. Kayci, A. Radenovic, and A. Kis, "Ultrasensitive photodetectors based on monolayer MoS_2," *Nature Nanotechnol.*, vol. 8, no. 7, pp. 497–501, Jul. 2013.

[3] M.-L. Tsai *et al.*, "Monolayer MoS_2 heterojunction solar cells," *ACS Nano*, vol. 8, no. 8, pp. 8317–8322, Aug. 2014.

[4] A. Srivastava, M. Sidler, A. V. Allain, D. S. Lembke, A. Kis, and A. Imamoglu, "Optically active quantum dots in monolayer WSe_2," *Nature Nanotechnol.*, vol. 10, no. 6, pp. 491–496, 2015.

[5] C. Palacios-Berraquero *et al.*, "Large-scale quantum-emitter arrays in atomically thin semiconductors," *Nature Commun.*, vol. 8, no. 1, pp. 1–6, Aug. 2017.

[6] K. Barthelmi *et al.*, "Atomistic defects as single-photon emitters in atomically thin MoS_2," *Appl. Phys. Lett.*, vol. 117, no. 7, Aug. 2020, Art. no. 070501.

[7] A. Splendiani *et al.*, "Emerging photoluminescence in monolayer MoS_2," *Nano Lett.*, vol. 10, no. 4, pp. 1271–1275, 2010.

[8] A. Chernikov *et al.*, "Exciton binding energy and nonhydrogenic Rydberg series in monolayer WS_2," *Phys. Rev. Lett.*, vol. 113, no. 7, Aug. 2014, Art. no. 076802.

[9] J. R. Schaibley *et al.*, "Valleytronics in 2D materials," *Nature Rev. Mater.*, vol. 1, no. 11, pp. 1–15, Nov. 2016.

[10] R. Frisenda *et al.*, "Recent progress in the assembly of nanodevices and van der Waals heterostructures by deterministic placement of 2D materials," *Chem. Soc. Rev.*, vol. 47, no. 1, pp. 53–68, Jan. 2018.

[11] A. Reserbat-Plantey *et al.*, "Strain superlattices and macroscale suspension of graphene induced by corrugated substrates," *Nano Lett.*, vol. 14, no. 9, pp. 5044–5051, Sep. 2014.

[12] J. Chaste *et al.*, "Intrinsic properties of suspended MoS_2 on SiO_2/Si pillar arrays for nanomechanics and optics," *ACS Nano*, vol. 12, no. 4, pp. 3235–3242, Apr. 2018.

[13] A. Branny, S. Kumar, R. Proux, and B. D. Gerardot, "Deterministic strain-induced arrays of quantum emitters in a two-dimensional semiconductor," *Nature Commun.*, vol. 8, no. 1, pp. 1–7, Aug. 2017.

[14] M. Vutukuru, H. Ardekani, Z. Chen, R. L. Wilmington, K. Gundogdu, and A. K. Swan, "Enhanced dielectric screening and photoluminescence from nanopillar-strained MoS_2 nanosheets: Implications for strain funneling in optoelectronic applications," *ACS Appl. Nano Mater.*, vol. 4, no. 8, pp. 8101–8107, 2021.

[15] F. Dirnberger *et al.*, "Quasi-1D exciton channels in strain-engineered 2D materials," *Sci. Adv.*, vol. 7, no. 44, Oct. 2021, Art. no. eabj3066.

[16] M. Buscema, G. A. Steele, H. S. J. van der Zant, and A. Castellanos-Gomez, "The effect of the substrate on the Raman and photoluminescence emission of single-layer MoS_2," *Nano Res.*, vol. 7, no. 4, pp. 561–571, Apr. 2014.

[17] J. Feng, X. Qian, C.-W. Huang, and J. Li, "Strain-engineered artificial atom as a broad-spectrum solar energy funnel," *Nature Photon.*, vol. 6, no. 12, pp. 866–872, Nov. 2012.

[18] M. G. Harats, J. N. Kirchhof, M. Qiao, K. Greben, and K. I. Bolotin, "Dynamics and efficient conversion of excitons to trions in non-uniformly strained monolayer WS_2," *Nature Photon.*, vol. 14, no. 5, pp. 324–329, May 2020.

[19] O. Iff *et al.*, "Substrate engineering for high-quality emission of free and localized excitons from atomic monolayers in hybrid architectures," *Optica*, vol. 4, no. 6, p. 669, Jun. 2017.

[20] L. Güniat, P. Caroff, and A. F. I. Morral, "Vapor phase growth of semiconductor nanowires: Key developments and open questions," *Chem. Rev.*, vol. 119, no. 15, pp. 8958–8971, Aug. 2019.

[21] W. Kim, L. Güniat, A. F. I. Morral, and V. Piazza, "Doping challenges and pathways to industrial scalability of III–V nanowire arrays," *Appl. Phys. Rev.*, vol. 8, no. 1, Mar. 2021, Art. no. 011304.

[22] J. Vukajlovic-Plestina *et al.*, "Engineering the size distributions of ordered GaAs nanowires on silicon," *Nano Lett.*, vol. 17, no. 7, pp. 4101–4108, Jul. 2017.

[23] J. Vukajlovic-Plestina *et al.*, "Fundamental aspects to localize self-catalyzed III–V nanowires on silicon," *Nature Commun.*, vol. 10, no. 1, p. 869, Dec. 2019.

[24] F. Matteini, G. Tütüncüoglu, H. Potts, F. Jabeen, and A. F. I. Morral, "Wetting of Ga on SiO_x and its impact on GaAs nanowire growth," *Cryst. Growth Des.*, vol. 15, no. 7, pp. 3105–3109, Jul. 2015.

[25] C. Lee, H. Yan, L. E. Brus, T. F. Heinz, J. Hone, and S. Ryu, "Anomalous lattice vibrations of single- and few-layer MoS_2," *ACS Nano*, vol. 4, no. 5, pp. 2695–2700, May 2010, doi: 10.1021/nn1003937.

[26] M. A. Giambra *et al.*, "Wafer-scale integration of graphene-based photonic devices," *ACS Nano*, vol. 15, no. 2, pp. 3171–3187, Feb. 2021.

[27] H. Yu *et al.*, "Wafer-scale growth and transfer of highly-oriented monolayer MoS_2 continuous films," *ACS Nano*, vol. 11, no. 12, pp. 12001–12007, Dec. 2017.

[28] K.-K. Liu *et al.*, "Growth of large-area and highly crystalline MoS_2 thin layers on insulating substrates," *Nano Lett.*, vol. 12, no. 3, pp. 1538–1544, Mar. 2012.

[29] A. C. Ferrari, "Raman spectroscopy of graphene and graphite: Disorder, electron–phonon coupling, doping and nonadiabatic effects," *Solid State Commun.*, vol. 143, nos. 1–2, pp. 47–57, Jul. 2007.

[30] X. Zhang, X.-F. Qiao, W. Shi, J.-B. Wu, D.-S. Jiang, and P.-H. Tan, "Phonon and Raman scattering of two-dimensional transition metal dichalcogenides from monolayer, multilayer to bulk material," *Chem. Soc. Rev.*, vol. 44, no. 9, pp. 2757–2785, 2015.

[31] D. Lloyd *et al.*, "Band gap engineering with ultralarge biaxial strains in suspended monolayer MoS_2," *Nano Lett.*, vol. 16, no. 9, pp. 5836–5841, Sep. 2016.

[32] B. Chakraborty, A. Bera, D. V. S. Muthu, S. Bhowmick, U. V. Waghmare, and A. K. Sood, "Symmetry-dependent phonon renormalization in monolayer MoS_2 transistor," *Phys. Rev. B, Condens. Matter*, vol. 85, no. 16, Apr. 2012, Art. no. 161403.

[33] A. Molina-Sanchez and L. Wirtz, "Phonons in single-layer and few-layer MoS_2 and WS_2," *Phys. Rev. B, Condens. Matter*, vol. 84, no. 15, Oct. 2011, Art. no. 155413.

[34] T. L. Atallah *et al.*, "Electrostatic screening of charged defects in monolayer MoS_2," *J. Phys. Chem. Lett.*, vol. 8, no. 10, pp. 2148–2152, May 2017.

[35] J. W. Christopher, B. B. Goldberg, and A. K. Swan, "Long tailed trions in monolayer MoS_2: Temperature dependent asymmetry and resulting red-shift of trion photoluminescence spectra," *Sci. Rep.*, vol. 7, no. 1, pp. 1–8, Dec. 2017.

[36] E. Mitterreiter *et al.*, "The role of chalcogen vacancies for atomic defect emission in MoS_2," *Nature Commun.*, vol. 12, no. 1, pp. 1–8, Dec. 2021.

[37] H. J. Conley, B. Wang, J. I. Ziegler, R. F. Haglund, S. T. Pantelides, and K. I. Bolotin, "Bandgap engineering of strained monolayer and bilayer MoS_2," *Nano Lett.*, vol. 13, no. 8, pp. 3626–3630, Aug. 2013.

[38] Y. Lin *et al.*, "Dielectric screening of excitons and trions in single-layer MoS_2," *Nano Lett.*, vol. 14, no. 10, pp. 5569–5576, Oct. 2014.

[39] A. Raja *et al.*, "Coulomb engineering of the bandgap and excitons in two-dimensional materials," *Nature Commun.*, vol. 8, no. 1, pp. 1–7, Aug. 2017.

[40] H. Nan *et al.*, "Strong photoluminescence enhancement of MoS_2 through defect engineering and oxygen bonding," *ACS Nano*, vol. 8, no. 6, pp. 5738–5745, Jun. 2014.

[41] W. Su, H. Dou, J. Li, D. Huo, N. Dai, and Li Yang, "Tuning photoluminescence of single-layer MoS_2 using H_2O_2," *RSC Adv.*, vol. 5, no. 101, pp. 82924–82929, 2015.

[42] W. J. Moore and R. T. Holm, "Infrared dielectric constant of gallium arsenide," *J. Appl. Phys.*, vol. 80, no. 12, pp. 6939–6942, Dec. 1996.

[43] S. M. Sze and K. K. Ng, *Physics of Semiconductor Devices*. Hoboken, NJ, USA: Wiley, 2006.

[44] Y. J. Noori *et al.*, "Photonic crystals for enhanced light extraction from 2D materials," *ACS Photon.*, vol. 3, no. 12, pp. 2515–2520, Dec. 2016.

[45] M. E. Reimer *et al.*, "Bright single-photon sources in bottom-up tailored nanowires," *Nature Commun.*, vol. 3, no. 1, pp. 1–6, Jan. 2012.
[46] M. Heiss *et al.*, "Self-assembled quantum dots in a nanowire system for quantum photonics," *Nat. Mater.*, vol. 12, no. 5, pp. 439–444, Feb. 2013.
[47] I. Friedler, C. Sauvan, J. P. Hugonin, P. Lalanne, J. Claudon, and J. M. Gérard, "Solid-state single photon sources: The nanowire antenna," *Opt. Exp.*, vol. 17, no. 4, p. 2095, 2009.
[48] A. Balgarkashi *et al.*, "Facet-driven formation of axial and radial In(Ga)As clusters in GaAs nanowires," *J. Opt.*, vol. 22, no. 8, Aug. 2020, Art. no. 084002.
[49] A. Castellanos-Gomez *et al.*, "Deterministic transfer of two-dimensional materials by all-dry viscoelastic stamping," *2D Mater.*, vol. 1, no. 1, Apr. 2014, Art. no. 011002.

Akshay Balgarkashi received the B.E. degree in electronics engineering from the University of Mumbai, India, in 2012, and the M.Tech. degree in electronics engineering (microelectronics) from the Indian Institute of Technology, Mumbai, India, in 2016. He is currently pursuing the Ph.D. degree with the Department of Materials Science and Engineering, École Polytechnique Fédérale de Lausanne (EPFL), Lausanne, Switzerland. His research interests include epitaxial growth and characterization of semiconductor nanostructures and integration with 2D materials.

Valerio Piazza received the M.Sc. degree in materials engineering and nanotechnology from the Politecnico di Milano, Italy, in 2015, and the Ph.D. degree in nanoscale characterization of III–V nanowires from Université Paris Sud, France, in 2018. He is the Winner of the Piaget Scientific Award 2020. He is currently a Post-Doctoral Researcher with the Department of Materials Science, Ecole Polytechnique Fédérale de Lausanne. His current research interests include the epitaxial growth of compound semiconductors, characterization of fundamental properties of low-dimensional systems, and device fabrication.

Jakub Jasiński is currently pursuing the Ph.D. degree with the Doctoral School, Wrocław University of Science and Technology, in the field of solid-state physics at the Quantum Electronics Group led by Paulina Płochocka. He is realizing his Ph.D. studies within a Preludium Bis Project titled "Toward deterministic control of van der Waals heterostructures properties." As part of his doctoral work, he is doing research on fundamental properties of two-dimensional Transition Metal Dichalcogenides using various optical spectroscopy techniques.

Riccardo Frisenda received the B.Sc. and M.Sc. degrees in physics from La Sapienza University, Roma, Italy, and the Ph.D. degree in molecular electronics from the Technical University of Delft, Delft, The Netherlands. After earning his Ph.D. degree, in 2016, he joined as a Post-Doctoral Researcher with the Andres Castellanos' Research Group, Madrid, Spain, first in IMDEA Nanoscience and later in ICMM-CSIC, in 2018. His research interests deal with transport at the nanoscale, electronic and optoelectronic propertied of 2D materials, and the physics of devices based on them.

Alessandro Surrente received the Ph.D. degree in physics from the École Polytechnique Fédérale de Lausanne, Switzerland, in 2013. He worked on the epitaxial growth and optical properties of position-controlled semiconductor quantum dots with the École Polytechnique Fédérale de Lausanne. He has worked as a Post-Doctoral Fellow at CNRS. He was awarded an individual Marie Skłodowska-Curie Fellowship, which funded his stay at Sapienza University, Rome, Italy. He is currently an Assistant Professor with the Wrocław University of Science and Technology, Poland. His current research are devoted to the investigation of the optical properties of layered materials and metal halide perovskites via optical spectroscopy, both at zero and very high magnetic fields.

Michał Baranowski has been an Assistant Professor with the Department of Experimental Physics, Wrocław University of Science and Technology, since 2015. From 2016 to 2019, he was a Visiting Scientist at LNCMI-CNRS Toulouse, working with the Head of the Quantum Electronics Group Paulina Plochocka. His main scientific interest is optical spectroscopy of emerging semiconducting materials. In the last years, his activity has been focused on the rapidly expanding research fields of 2D materials and metal-halide perovskites.

Mirjana Dimitrievska received the bachelor's and master's degrees from the University of Novi Sad, Serbia and the Ph.D. degree in physics from the University of Barcelona, Spain. She is currently a Materials Scientist with the École polytechnique fédérale de Lausanne (EPFL). Afterwards, she moved to USA, where she was working as a Research Scientist with the National Renewable Energy Laboratory (NREL) and the National Institute of Standards and Technology (NIST). In 2020, she moved to Switzerland and joined EPFL. Her research are focused on discovering and optimizing functional materials for solar cells and solid-state battery applications.

Didem Dede received the B.Sc. degree in metallurgical and materials engineering from Middle East Technical University in 2016 and the M.Sc. degree in materials science from the National Nanotechnology Research Center, Bilkent University, in 2018. She is currently pursuing the Ph.D. degree with the Department of Materials Science and Engineering, École Polytechnique Fédérale de Lausanne (EPFL). Her research focuses on the epitaxial growth III–V horizontal nanowires and their structural characterization.

Wonjong Kim received the B.S. degree from the Department of Information Display, Kyung Hee University, South Korea, in 2014, the dual master's degree from the Department of Information Display, Kyung Hee University and in innovation technologique: ingénierie et entrepreneuriat from the Ecole Polytechnique, France, in 2017, and the Ph.D. degree in material science and engineering from the École Polytechnique Fédérale de Lausanne, Switzerland, in 2020. He is currently working at ASM International as a Senior Process Engineer. His research interests are epitaxial deposition of silicon and silicon germanium for applications in the areas of logic and memory.

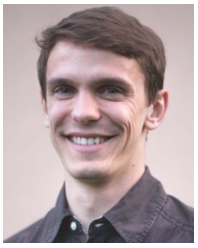

Lucas Güniat received the master's degree in materials science and engineering from EPFL in 2016 and the Ph.D. degree in 2021 with a focus on whether III–V integration on Si can be done using vertical nanostructures. After his master's thesis work on Ge nanowires with the McIntyre Group, Stanford University. His interest in epitaxy and nanostructure fabrication lead him to start a Ph.D. at EPFL, Laboratory of Semiconductor Materials (LMSC—Professor Anna Fontcuberta i Morral) on the kinetics of III–V semiconductor nanowire growth on Si.

Jean-Baptiste Leran received the master's degree in mechanical engineering from Conservatoire National des Arts et Métiers, Aix-en Provence/Paris, France. Before obtaining his master's degree, he worked several years at Thales Alenia Space, Cannes, France, in the field of satellite testing. He moved to École Polytechnique Fédérale de Lausanne (EPFL), Lausanne, Switzerland, as a Scientific Collaborator. He is currently a Molecular Beam Epitaxy Expert.

Andres Castellanos-Gomez is currently a Tenured Scientist with the Spanish National Research Council (Consejo Superior de Investigaciones Científicas, CSIC). He explores novel 2D materials and studies their mechanical, electrical, and optical properties with special interest on the application of these materials in nanomechanical and optoelectronic devices. He is the author of 150 articles in international peer-reviewed journals and six book chapters. He is the Principal Investigator of a prestigious ERC Starting Grant. Among other recognitions, he has been appointed as a fellow of the International Association of Advanced Materials (IAAM) in 2020. He has been included in the Highly Cited Researchers 2018, 2019, and 2020 lists of Clarivate/WOS. He has been also recognized with the Young Researcher Award (experimental physics) of the Royal Physical Society of Spain (2016).

Paulina Plochocka is currently the Directrice de Recherché de 2e classe (DR2) with the Laboratoire National des Champs Magnétiques Intenses (LNCMI), CNRS, Toulouse; and a part-time Professor with the Department of Experimental Physics, Faculty of Fundamental Problems of Technology, Wrocław University of Science and Technology, Poland. Her career started at Warsaw University, where she defended her Ph.D. degree. After she worked as a Post-Doctoral Researcher with the Weizmann Institute, where she studied the Quantum Hall effect. In 2006, she moved to LNCMI-CNRS Grenoble. In 2011, she created the Quantum Electronics Group. The group investigates the properties of emerging layered semiconductors under extreme conditions of high magnetic field and low temperatures.

Anna Fontcuberta i Morral (Member, IEEE) received the degree in physics from the University of Barcelona and the Ph.D. degree in materials science from Ecole Polytechnique, France.

She is currently a Full Professor in materials science and engineering and in physics and the Associate Vice-President of Centers and Platforms at EPFL. She is a member of the EPFL-WISH Foundation and a Former President of the foundation, whose goal is to support female students on accomplishing their professional dreams. She performed post-doctoral research at CalTech with Prof. Harry Atwater, with whom she also co-founded the start-up company Aonex Technologies. After a brief period as a CNRS Researcher at Ecole Polytechnique, she moved to TU Munich (Walter Schottky Institut) as a Group Leader. She has been a Professor at EPFL, since 2008. Among the awards, she has received are the Marie Curie Excellence Grant, ERC Starting Grant, the SNSF-Backup Schemes Consolidator Grant, and the EPS Emy Noether Prize.